

Electronic states realized by the interplay between Li diffusion and $\text{Co}^{3+}/\text{Co}^{4+}$ charge ordering in Li_xCoO_2

Kiyotaka Miyoshi,¹ Kentaro Manami,¹ Ryo Sasai,¹ Shijo Nishigori,² and Jun Takeuchi¹

¹*Department of Material Science, Shimane University, Matsue 690-8504, Japan and*

²*Department of Materials Analysis, CIRIS, Shimane University, Matsue 690-8504, Japan*

(Dated: November 5, 2018)

Measurements of dc magnetization (M) and electrical resistivity (ρ) have been carried out as a function of temperature (T) for layered oxide Li_xCoO_2 ($0.51 \leq x \leq 1.0$) using single crystal specimens. After slow cooling of the specimens down to 10 K, both of the $M(T)$ and $\rho(T)$ curves are found to exhibit a clear anomaly due to the occurrence of $\text{Co}^{3+}/\text{Co}^{4+}$ charge ordering (CO) at $T_S \sim 155$ K for $0.6 \leq x \leq 0.98$ (at $T_S \sim 180$ – 190 K for $0.5 \leq x \leq 0.55$). After rapid cool of the specimens, additional anomalies are observed related to the onset of Li diffusion at $T_{F1} \sim 370$ K and/or $T_{F2} \sim 120$ – 130 K. Due to phase mixing with compositions of nearly LiCoO_2 and $\text{Li}_{2/3}\text{CoO}_2$, the specimens with $0.7 \lesssim x \lesssim 0.9$ show anomalies both at T_{F1} and T_{F2} . For $0.6 \lesssim x \lesssim 0.9$, the resistivity measured after rapid cooling is found to be fairly larger than that measured after slow cooling below T_S . The enhanced resistivity can be explained by the scenario that disordered $\text{Co}^{3+}/\text{Co}^{4+}$ arrangements, which have been observed and revealed to have an insulating electronic structure contrasting to the regular CO state in the previous scanning tunneling microscopy measurements [Phys. Rev. Lett. **111**, 126104 (2013)], are realized due to the formation of an amorphous-like structure of Li ions after rapid cooling via interlayer Coulomb coupling. An electronic phase diagram for $0.5 \leq x \leq 1.0$ is proposed.

PACS numbers:

I. INTRODUCTION

Li-ion batteries are now being widely used for mobile electronic devices and also electric vehicles, and have been the subject of intensive study to improve storage capacity and longevity.^{1,2} One of the most common cathode materials used in commercial Li-ion batteries with high-energy density and a proper application voltage is layered oxide Li_xCoO_2 , in which both Li and Co atoms are octahedrally coordinated by oxygen atoms, forming a two-dimensional (2D) regular triangular lattice in each layer, and each layer is alternatively stacked along the c -axis. Much attention has been focused on the high mobility of Li ions in Li_xCoO_2 for the application but various unconventional physical natures are expected as in the related material Na_xCoO_2 , which has a similar structure consisting of Na and CoO_2 layers. Indeed, Na_xCoO_2 has been under intensive study for the past two decades due to the various intriguing electronic properties, such as a large thermoelectric power ($x \sim 0.7$),³ superconductivity ($T_c \sim 5$ K) in the hydrated compound ($x \sim 0.35$),⁴ an insulating ground state induced by charge ordering ($x \sim 0.5$),^{5–8} a mass-enhanced Fermi-liquid ground state analogous to LiV_2O_4 ,⁹ a spin-density-wave state,¹⁰ in addition to the characteristic Na order,^{11–22} which has been found to be linked with $\text{Co}^{3+}/\text{Co}^{4+}$ charge disproportionation,^{14–19} magnetic ordering,^{20,22} and structural transitions.²¹

In both compounds, Co ions are in a mixed valence state consisting of Co^{3+} (t_{2g}^6) and Co^{4+} (t_{2g}^5) having spins of $S=0$ and $S=1/2$, respectively,²³ since the deintercalation of Li or Na ions from the mother compounds generates Co^{4+} on the 2D triangular lattice of Co^{3+} . Thus, a hole doping in the t_{2g} orbital can be made by the deintercalation in Li_xCoO_2 , where the electrical re-

sistivity drastically decreases and a metallic behavior appears in the $\rho(T)$ curve with decreasing x from 1.0 to 0.9.^{24–28} One of the most characteristic features of Li_xCoO_2 is the $\text{Co}^{3+}/\text{Co}^{4+}$ charge ordering (CO), which has been inferred from sharp anomalies observed in the dc magnetization,^{25,29–32} resistivity^{26,27}, and specific heat²⁶ data at $T_S = 150$ – 170 K in wide range of x , and found to have a characteristic $\sqrt{3} \times \sqrt{3} R30^\circ$ arrangement of Co^{4+} by recent scanning tunneling microscopy (STM) observations and density functional theory (DFT) calculations.³³

The ordering of $\text{Co}^{3+}/\text{Co}^{4+}$ can be strongly affected by the dynamics of Li ions via interlayer Coulomb coupling. In a previous study, we have reported that the dc magnetization (M) versus temperature (T) curve measured after rapid cooling of the specimens is different from that measured after slow cooling below $T_F \sim 120$ K for $x = 0.66$,²⁶ suggesting that Li ions stop diffusing and become ordered below T_F , since T_F is similar to T_{MN} and T_d^{Li} determined by the measurements of NMR³⁴ and muon spin rotation (μSR)³⁵, respectively, as the temperature below which Li ions start diffusing. The origin of the difference below T_F is attributed to the difference in the $\text{Co}^{3+}/\text{Co}^{4+}$ arrangement, which is expected to be disordered when the Li ions form an amorphous-like structure as in a glassy state after a rapid cooling down to a temperature far below T_F . Indeed, it has been revealed in the previous STM observations at $T \sim 5$ K for $\text{Li}_{0.66}\text{CoO}_2$ that there is some disordered area on the crystal surface where the CO state is destroyed and an insulating gap in the dI/dV spectrum is detected. Thus, the cooling-rate-dependent Li ordering might play a decisive role in determining the $\text{Co}^{3+}/\text{Co}^{4+}$ arrangement.

High-quality single-crystal specimens of Li_xCoO_2 used in the previous study have enabled us to understand the electronic properties through microscopic

measurements^{33,36–39}, but the interplay between Li diffusion and $\text{Co}^{3+}/\text{Co}^{4+}$ ordering, and the evolution of the charge ordering for the delithiation have remained unsolved. In the present paper, we have performed dc magnetization and electrical resistivity measurements for Li_xCoO_2 using single-crystal specimens with a systematic change of Li content x ($0.5 \leq x \leq 1.0$) to shed further light on the problems. It has been found that electrical resistivity for the specimens with $0.6 \lesssim x \lesssim 0.9$ measured after rapid cooling of the specimens becomes much larger than that measured after slow cooling below $T_S \sim 155$ K. The results are consistent with the above-mentioned scenario that the region where the CO state is destroyed, having an insulating electronic structure, appears due to the amorphous-like structures in the Li layers induced by the rapid cooling. We have proposed an electronic phase diagram for $0.5 \leq x \leq 1.0$ based on the results of the measurements using 12 single-crystal specimens with different x .

II. EXPERIMENT

Single crystal specimens of Li_xCoO_2 ($0.51 \leq x \leq 1.0$) were obtained by chemically delithiating from LiCoO_2 single-crystals, as described in a previous report.²⁶ In the first step, single crystals of $\text{Na}_{0.75}\text{CoO}_2$ were grown in an optical floating-zone furnace in a similar manner as described in the literature.⁴⁰ The obtained single crystal rods of $\text{Na}_{0.75}\text{CoO}_2$ were crushed into small pieces, and then cleaved into thin slices with a thickness of ~ 0.2 mm. In the next step, to obtain LiCoO_2 single crystals by ion exchange reactions, the cleaved $\text{Na}_{0.75}\text{CoO}_2$ single crystals were embedded in Li_2CO_3 powder in an alumina boat, and heated 600 °C for 24 h in air, and then repeatedly washed with acetonitrile to remove Li_2CO_3 and Na_2CO_3 . After annealing these crystals at 900 °C for 24 h in air, single crystal specimens of pristine LiCoO_2 were obtained, which have a plate-like shape with a typical dimension of $2 \times 2 \times 0.2$ mm³. In the final step, the delithiation from pristine LiCoO_2 crystals was carried out by chemically extracting lithium using NO_2BF_4 as the oxidizer. The reaction was carried out in an argon atmosphere by immersing LiCoO_2 crystals in an acetonitrile solution of NO_2BF_4 and heating at 50 °C for 72 h in a pressure vessel with a Teflon liner, and finally washed to remove LiBF_4 by acetonitrile. The Li content x ($0.51 \leq x \leq 1.0$) in the crystals was controlled by the molar ratio between LiCoO_2 and NO_2BF_4 ranging from 1 : 0 ($x=1.0$) to 1 : 1.5 ($x=0.51$), and was determined by inductively coupled plasma atomic emission spectroscopy (ICP-AES) using a Perkin-Elmer Optima 2000 DV instrument. For all specimens, a part of the single crystal was crushed into powder and the phase purity of the specimens was confirmed by powder x-ray diffraction (XRD) measurements with a 2θ range from 10° to 90° using a Rigaku RINT2200 diffractometer with $\text{Cu } K\alpha$ radiation. Almost all of the peaks were found to be ascribed to the Li_xCoO_2 compound. XRD patterns of some specimens

prepared by the same procedures for $10^\circ \leq 2\theta \leq 90^\circ$ can be seen in the previous report.²⁶ dc magnetization measurements were performed by a Quantum Design magnetic property measurement system (MPMS). Electrical resistivity was measured by a standard four-probe technique. For the resistivity measurements, specimens were cooled by using a Gifford-McMahon (GM) refrigerator or a cryostat of the MPMS.

III. RESULTS AND DISCUSSION

A. Powder x-ray diffraction

The phase mixing of two hexagonal structures had been observed earlier in Li_xCoO_2 for $0.75 < x < 0.90$ through XRD measurements.^{24,32,41–44} To investigate the evolution of the phase separation with decreasing x , we focus here on the (003) reflection observed in the powder XRD measurements. As shown in Fig. 1(a), we observe a (003) peak accompanied by a shoulder at the lower angle side for $x=0.83$ and 0.88 , corresponding to the phase separation, but a (003) single peak for $0.96 \leq x \leq 1.0$. Also, we observe a double peak for $x=0.73$ and 0.75 but a single peak again for $x \leq 0.64$. As shown in Fig. 1(b), we can extract two components from the peak for $0.71 \leq x \leq 0.91$. We assign the component with a smaller (larger) lattice constant c as the hexagonal phase (I) [hexagonal phase (II)], which has higher (lower) Li content.⁴⁵ In Fig. 1(c), the lattice constant c is plotted as a function of x . Furthermore, we estimated the molar fraction of the hexagonal phase (I) ($=p^I$) and (II) ($=p^{II}$) for each x from the integrated intensity of the peak. The results are plotted in Fig. 1(d), where it is shown that the system evolves from phase (I) to phase (II) with decreasing x via the phase mixing state for $0.65 < x < 0.95$. The variation of p^I and p^{II} shown in Fig. 1(d) is consistent with that observed in an earlier work.⁴⁴

Here, we discuss the composition of the hexagonal phases (I) and (II). It is interesting to note that a small anomaly at T_S which indicates the emergence of the CO state is observed even for a slightly delithiated specimen with $x=0.98$ in the electrical resistivity and dc magnetization data, as seen later in Figs. 2(b) and 3(b). These behaviors let us imagine a simple situation that phases (I) and (II) are composed of LiCoO_2 ($x=1.0$) and $\text{Li}_{2/3}\text{CoO}_2$, respectively, and in the latter the CO state emerges below $T_S \sim 155$ K. Assuming this, the molar fraction of phases (I) and (II) can be given by the dashed lines shown in Fig. 1(d). Although the evolution of the molar fraction with decreasing x is quadratic rather than linear, the end of the mixing state appears to be at around $x=2/3$ as well as the simple model described by the dotted lines. Thus, for $0.9 < x < 1.0$, it is likely that a part of the introduced Co^{4+} ions by the delithiation develops $\text{Li}_{2/3}\text{CoO}_2$ domains [phase (II)], while the rest provides holes to the LiCoO_2 ($x=1.0$) region [phase (I)], leading to a rapid decrease in electrical resistivity with decreasing x , as seen

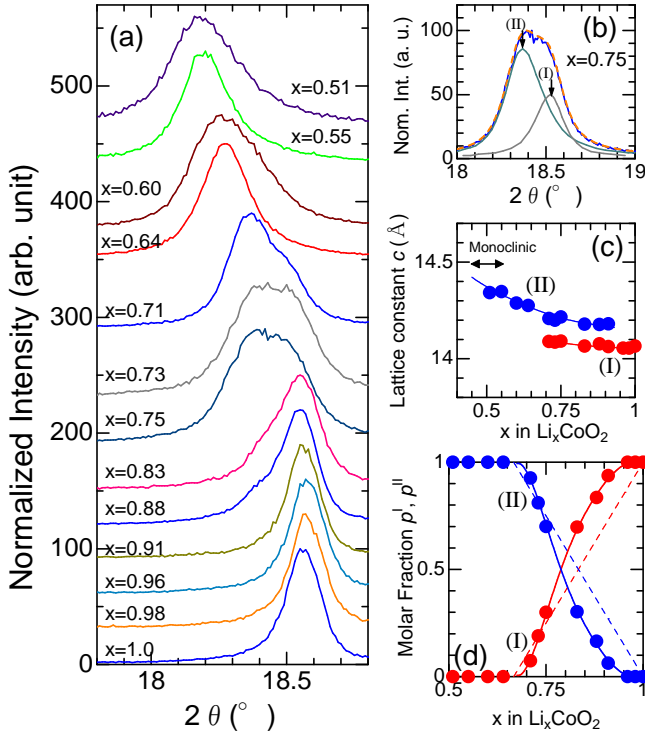


FIG. 1: (Color online) (a) 003 reflection peaks for Li_xCoO_2 ($0.51 \leq x \leq 1.0$) in powder x-ray diffraction. (b) A typical 003 split peak observed due to the phase separation in the specimen with $x=0.75$. Two peaks can be extracted from the split peak. Each peak corresponds to a hexagonal structure [(I) or (II)] with different lattice parameters. (c) Lattice parameters c for Li_xCoO_2 plotted as a function of x . The solid lines are guide for the eyes. The crystal structure transforms from hexagonal (I) to hexagonal (II) with decreasing x . A monoclinic phase is known to appear in the neighborhood of $x=0.5$ ⁴³. (d) Molar fraction of hexagonal phase (I) and (II) in Li_xCoO_2 estimated from the ratio of the integrated intensity of the 003 peak. The solid lines are guide for the eyes. The dashed lines indicate the calculated molar fraction of LiCoO_2 (red lines) and $\text{Li}_{2/3}\text{CoO}_2$ regions (blue line), assuming that the system is composed of the mixture of LiCoO_2 and $\text{Li}_{2/3}\text{CoO}_2$ for $2/3 < x < 1.0$.

later in Figs. 2(a)-2(c). The scenario explains why p^{II} increases slower than the dashed line as decreasing x . As discussed later, phases (I) and (II) can be regarded to have compositions of $x \sim 1.0$ and $x \sim 2/3$, respectively.

B. Electrical resistivity

We show the temperature dependence of electrical resistivity (ρ) for Li_xCoO_2 ($0.51 \leq x \leq 1.0$) in Figs. 2(a)-2(m). The data were collected during heating from ~ 10 K to room temperature after slow cooling of the specimens by using a GM refrigerator at an averaged cooling rate ~ -2 K/min. As seen in Fig. 2(a), the ρ - T curve for LiCoO_2 ($x=1.0$) shows an insulating behavior. The $\rho(T)$ curves for $x=0.98$ and 0.96 in Figs. 2(b) and

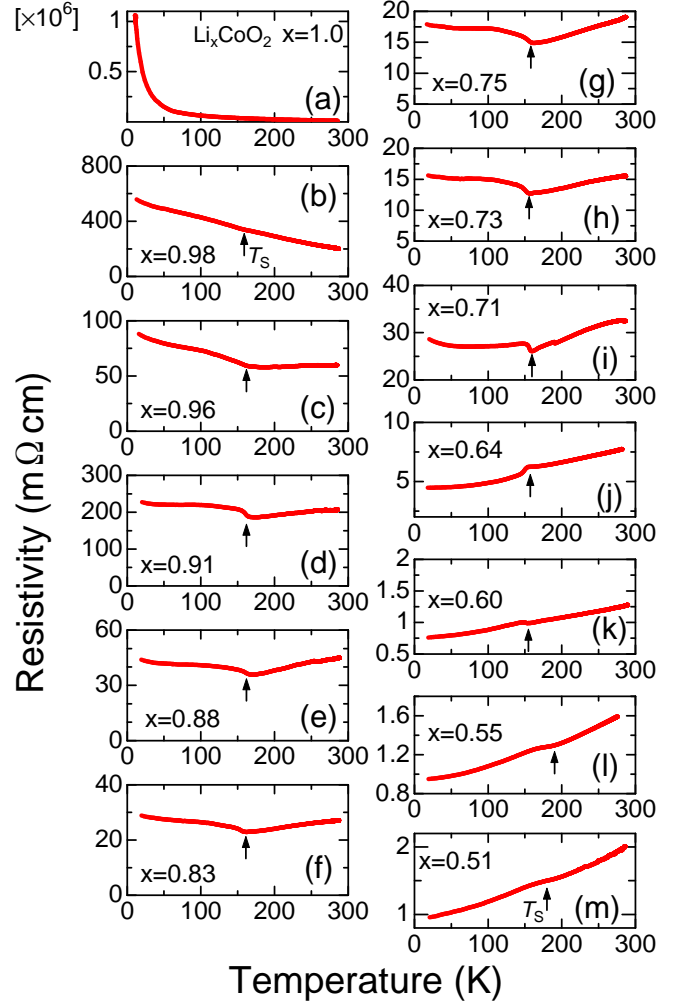


FIG. 2: (Color online) Temperature dependence of electrical resistivity ρ measured along the ab plane for Li_xCoO_2 with $x=1.0$ (a), 0.98 (b), 0.96 (c), 0.91 (d), 0.88 (e), 0.83 (f), 0.75 (g), 0.73 (h), 0.71 (i), 0.64 (j), 0.60 (k), 0.55 (l), 0.51 (m).

2(c) also show an insulating behavior but the amplitude of resistivity is fairly smaller than that for $x=1.0$. We should also note that both of the curves exhibit a slight anomaly at $T_S \sim 155$ K. These behaviors are consistent with the picture described in the previous section that the delithiation for $0.9 < x < 1.0$ gives rise to hole doping in the LiCoO_2 region [phase (I)] and also the construction of the $\text{Li}_{2/3}\text{CoO}_2$ domains [phase (II)], where the CO state appears below $T_S \sim 155$ K.

The $\rho(T)$ curves for $0.73 \leq x \leq 0.91$ show a qualitatively similar temperature dependence, which is metallic above T_S but insulating below T_S . In contrast, the $\rho(T)$ curve for $x \leq 0.64$ shows a metallic behavior above and below T_S . The metallic behavior below T_S is consistent with the results of the DFT calculation and the STM observation on the CO state, both of which have revealed the metallic electronic structure of the CO state.³³ The origin of the insulating behavior observed below T_S for $x \geq 0.73$ is unclear but is likely to be related to the fact that the

cobalt ions could not build a uniform CO state throughout the sample but a disordered one due to an excess of Co^{3+} for $x \geq 2/3$. As mentioned already, an insulating electronic structure has been revealed in the disordered CO state.³³ It should be also noted that T_S changes from 155 K for $0.60 \leq x \leq 0.98$ to 180-190 K for $x=0.51$ and 0.55. The different T_S values at $x \sim 1/2$ could be a signature of the formation of another $\text{Co}^{3+}/\text{Co}^{4+}$ arrangement with $\text{Co}^{3+} : \text{Co}^{4+} = 1 : 1$. Hereafter, we call the CO state with a formation of $\text{Co}^{3+} : \text{Co}^{4+} = 2 : 1$ and $1 : 1$ as the CO2/3 and CO1/2 states, respectively.

C. dc magnetization

In Figs. 3(a)-3(m), the temperature dependences of dc magnetization (M) measured in a magnetic field parallel to the ab plane under zero-field-cooled (ZFC) and field-cooled (FC) conditions for the specimens with $x=0.51-1.0$ are shown. The data were collected at first with increasing temperature from 10 K after rapid cooling of the specimens from 400 to 10 K in zero field, and then collected with increasing temperature after slow cooling at a cooling rate of -10 K/min from 400 K in a magnetic field of $H=1$ T and in zero field. For the rapid cooling, the specimens were quickly inserted in the chamber of a magnetometer kept at 10 K, after the specimens were taken from an oven heated above 400 K and quenched in acetonitrile to room temperature. The $M(T)$ curves for $x=1.0$ in Fig. 3(a) measured after slow cooling show a Curie-Weiss type paramagnetic behavior without any difference between the curves in the ZFC and FC conditions. The $\chi(T)$ [$=M(T)/H$] curves are fitted with the formula, $\chi = \chi_0 + C/(T - \Theta)$, yielding a constant susceptibility $\chi_0 = 7.93 \times 10^{-5}$ emu/mol/Oe, a Curie constant $C = 7.29 \times 10^{-3}$ emu/mol/K/Oe, and a Weiss temperature $\Theta = -4.80$ K. An effective magnetic moment per Co ions is given to be $\mu_{\text{eff}} = 0.241 \mu_B$, which is very small but is similar to that obtained in the previous work for $x=0.99$,²⁶ since Co^{3+} is supposed to be in the low spin state with $S=0$.

The $M(T)$ curve for $x=1.0$ measured after rapid cooling becomes different from those measured after slow cooling below $T_{F1} \sim 370$ K. The $M(T)$ curves for $x=0.98$ and 0.96 in Figs. 3(b) and 3(c) exhibit a slight anomaly at $T_S \sim 155$ K, in addition to the difference below T_{F1} . Furthermore, the $M(T)$ curves for $0.73 \leq x \leq 0.91$ in Figs. 3(d)-3(h) show an abrupt decrease below T_S , which is followed by an additional splitting below $T_{F2} \sim 120$ K. The $M(T)$ curves for $0.60 \leq x \leq 0.71$ in Figs. 3(i)-3(k) are similar to those observed for $0.73 \leq x \leq 0.91$ but have no difference below $T_{F1} \sim 370$ K. As mentioned in the Introduction, T_{F1} and T_{F2} are related to the temperatures, below which Li ions stop diffusing and order at the regular site. The difference in the amplitude of M is attributed to the difference in the ordering pattern of $\text{Co}^{3+}/\text{Co}^{4+}$, which depends on whether the Li ions sit on the regular site after slow cooling or exhibit amorphous-type order-

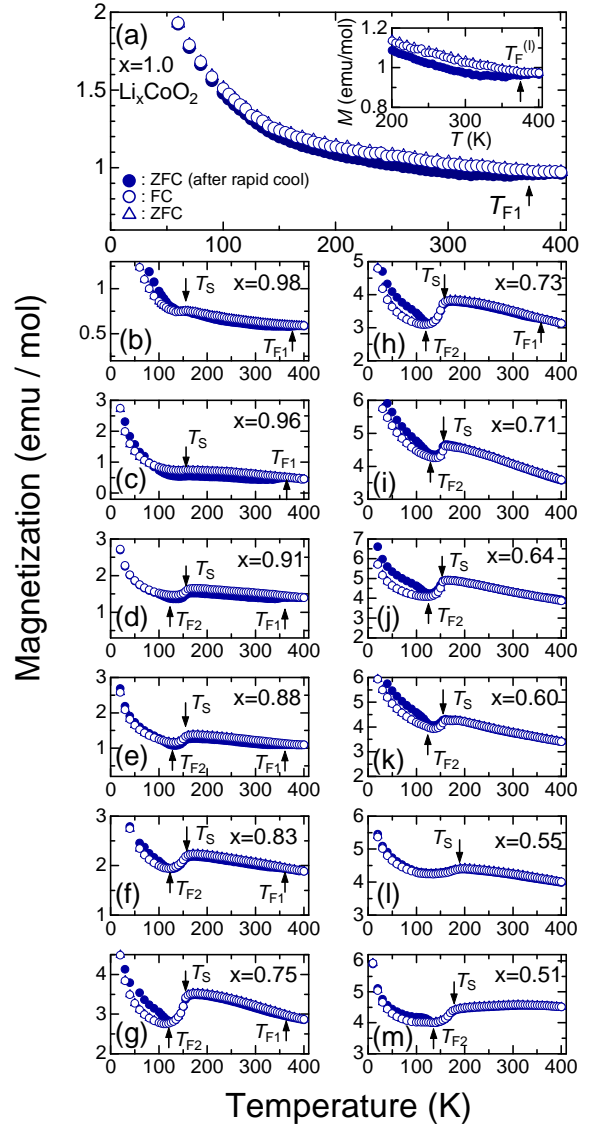


FIG. 3: (Color online) Temperature dependence of dc magnetization measured with a magnetic field of $H=1$ T parallel to the ab plane for Li_xCoO_2 with $x=1.0$ (a), 0.98 (b), 0.96 (c), 0.91 (d), 0.88 (e), 0.83 (f), 0.75 (g), 0.73 (h), 0.71 (i), 0.64 (j), 0.60 (k), 0.55 (l), 0.51 (m). The measurements were performed both after rapid cooling of the specimens from above 400 to 10 K in zero field (solid symbols) and after slow cooling down to 10 K in zero field and in a magnetic field of $H=1$ T (open symbols). The inset (a) shows a close-up of the $M(T)$ curve for $200 \leq T \leq 400$ K.

ing due to the glass-like freezing of Li^+ motions after rapid cooling.^{26,33} T_{F1} and T_{F2} seen in Figs. 3(a)-3(k) are thought to be related to the onset of the freezing of Li^+ motions in the hexagonal phase (I) with $x \sim 1.0$ and the phase (II) with $x \sim 2/3$, respectively. The x range for which anomalies are observed both at T_{F1} and T_{F2} is almost consistent with the nominal phase mixing region ($0.7 \lesssim x \lesssim 0.9$).

It is interesting to note that the amplitude of M mea-

sured after rapid cooling is enhanced below T_{F2} but coincides with the $M(T)$ curve measured after slow cooling above T_{F2} . The behavior appears to be remarkable for $0.60 \leq x \leq 0.83$. The enhancement of the amplitude of M below T_{F2} is consistent with the destruction of the CO2/3 state after rapid cooling, since the charge disordered state (liquid state) above T_S shows an enhanced amplitude compared with that below T_S . One may consider that the intermediate state between T_{F2} and T_S after rapid cooling is identical to the CO2/3 state realized after slow cooling. However, it will be seen later in Figs. 4(a) and 4(b) that those states may be similar but are not identical to each other. Another interesting feature is that the $M(T)$ curve for $x=0.55$ measured after rapid cooling in Fig. 3(l) shows a broad anomaly at $T_S \sim 190$ K, much higher than T_S of other specimens, and no visible anomaly at T_{F2} . The $M(T)$ curve for $x=0.51$, however, shows sharp anomalies at $T_S \sim 175$ K and $T_{F2} \sim 135$ K again, both of which are somewhat higher than those for $x \geq 0.60$. As noted in the previous section, the different T_S may denote an emergence of the CO1/2 state. The possible mechanism is discussed later.

D. Enhanced resistivity measured after rapid cooling

Previous STM observations at $T \sim 5$ K have revealed an insulating electronic structure in the region where disordered arrangements of $\text{Co}^{3+}/\text{Co}^{4+}$ ions are observed.³³ Therefore, in the case where Li ions have an amorphous-like disordered structure after rapid cooling, by which the CO2/3 state would be destroyed due to the interlayer Coulomb coupling, the electrical resistivity is expected to be extremely enhanced compared with that after slow cooling. Local distortions on the CoO_2 layers induced by the amorphous-like structure of the Li ions may also contribute to the destruction of the CO2/3 state. To confirm the behavior described above, we have examined the $\rho(T)$ curve after rapid cooling for some specimens. For the $\rho(T)$ measurements, we used a cryostat of the MPMS. Rapid cooling of the specimens was done by the rapid insertion of the sample rod in the chamber of the magnetometer kept at 10 K. The results are displayed in Figs. 4(a) and 4(b). As seen in the figures, the $\rho(T)$ curves measured after rapid cooling for $x=0.64$, 0.71 and 0.91 are found to be markedly enhanced compared with those after slow cooling below T_S . The enhancement of resistivity at 10 K attains 70% of the original value for $x=0.71$. Thus, we have certainly confirmed that Li ions probably enter an amorphous-like state after rapid cooling and destroy the CO2/3 state. A significant difference between the resistivity measured after slow and rapid cooling has been observed in some materials that undergo a metal-insulator transition. In these materials, a metastable high-temperature low-resistivity state are realized at low temperature by rapid cooling after pulsed laser heating.^{46,47} If our specimens are cooled

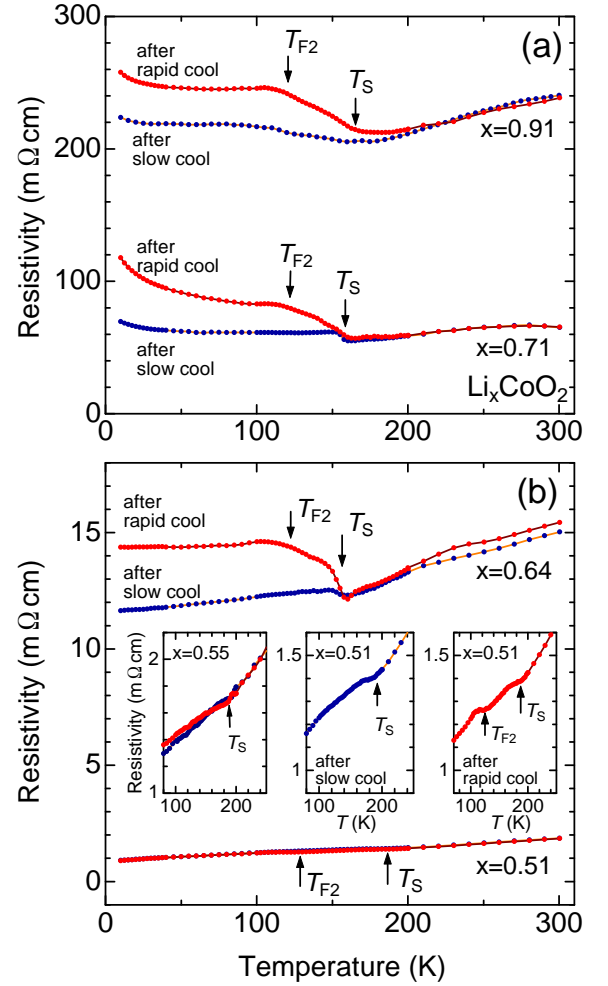


FIG. 4: (Color online) Temperature dependence of electrical resistivity measured along the ab plane for Li_xCoO_2 with (a) $x=0.91$ and 0.71 and (b) 0.64 and 0.51 . The measurements were performed both after slow cooling and rapid cooling of the specimens. The insets (b) show close-ups of the $\rho(T)$ curve for $x=0.51$ (right and center) and for $x=0.55$ (left).

more rapidly after local heating by pulsed laser radiation, the enhancement is expected to be more significant.

In contrast, for $x=0.51$, the $\rho(T)$ curve after rapid cooling is not enhanced compared with that after slow cooling, as shown in the insets (center and right) of Fig. 4(b). For $x=0.51$, an appearance of the CO1/2 state is expected but STM observations have never been conducted on the specimens with $x \sim 0.5$, so that the electronic properties of the state are unclear at the present stage. The results suggest either that the CO1/2 arrangement is not destroyed by the amorphous-like ordering of Li ions or that the arrangement is destroyed but the disordered state is also metallic. We also show the $\rho(T)$ curves for $x=0.55$ in the left inset of Fig. 4(b), where no anomaly is observed at T_{F2} in both curves, which is the same as the $M(T)$ curves for $x=0.55$ in Fig. 3(l). We should note here that all the $\rho(T)$ curves after rapid cool-

ing in Figs. 4(a) and 4(b) show an anomaly not only at T_S but also at $\sim T_{F2}$, showing a broad peak just below T_{F2} . On the other hand, $\rho(T)$ curves after slow cooling show an anomaly only at T_S . These features are consistent with those observed in the $M(T)$ curves. T_{F2} has been regarded as the temperature below which Li ions stop diffusing and enters into a solid state, since a characteristic splitting in the $M(T)$ curves has been observed depending on the cooling process below ~ 120 K.²⁶ However, the $\rho(T)$ curves in Figs. 4(a) and 4(b) exhibits a splitting below T_S , suggesting that Li ions start diffusing above T_S rather than T_{F2} . Considering the interlayer Coulomb coupling, it is more likely that the ordering of Li ions also enters a liquid state above T_S simultaneously with the transition of Co ions from the CO2/3 state to a charge liquid state. If so, what happens at T_{F2} ? Some amorphous metals, called metallic glasses, demonstrate a two-step transition from an amorphous glass state ($T < T_g$) to a liquid state ($T > T_x$) via an intermediate supercooled liquid state ($T_g < T < T_x$).^{48,49} One of the most exciting scenario is that the intermediate state between T_{F2} and T_S in Li_xCoO_2 is analogous to a supercooled liquid state observed in metallic glasses. To elucidate this, further investigations to confirm the thermodynamical properties by the measurements of specific heat and differential scanning calorimetry after rapid cooling of the specimens are desirable for a future study.

E. Ordering features and phase diagram

Here, we show the schematic image of the ordering in the Li and Co layers for $x=2/3$ at low temperatures in Fig. 5(a). Above T_S , Li ions can diffuse in the layers, and $\text{Co}^{3+}/\text{Co}^{4+}$ ions are in a charge liquid state. After slow cooling, Li^+ and Co^{3+} ions form a honeycomb lattice (HCL) below T_S , while Co^{4+} ions form a characteristic $\sqrt{3} \times \sqrt{3} R 30^\circ$ structure.³³ Contrasting to the regular structures after slow cooling, $\text{Co}^{3+}/\text{Co}^{4+}$ ions have a disordered arrangement after rapid cooling, as discussed in the previous section. Also, it is inferred that Li ions are frozen in an amorphous state from a liquid state by rapid cooling, leading to a disordered $\text{Co}^{3+}/\text{Co}^{4+}$ arrangement due to the interlayer Coulomb coupling. Amorphous structures in the Li layers have been also inferred for the specimen with $x=0.99$ to explain the large thermal history dependence in the $M(T)$ curve below ~ 380 K, which originates from the difference in the ordering pattern of Li ions depending on the cooling rate.²⁶ In the case that the Li site is fully occupied, the only way to give a different Li ordering pattern is to build an amorphous structure. For $T_{F2} \leq T \leq T_S$, we propose that the Li ions enter a supercooled liquid (SCL) state.

Next, we focus on the x dependences of T_{F1} , T_{F2} and T_S , which are summarized in Fig. 5(b). We notice that these temperatures are almost independent of x , suggesting that the hexagonal phase (I) [phase (II)] has a similar composition of LiCoO_2 ($\text{Li}_{2/3}\text{CoO}_2$) throughout

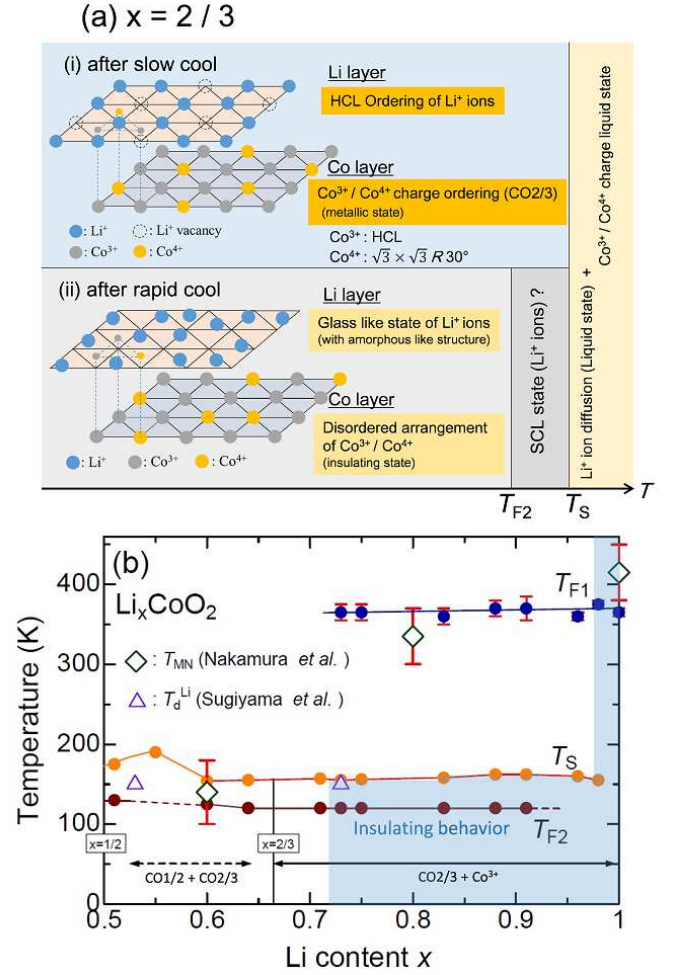


FIG. 5: (Color online) (a) Schematic image of the ordering in the Li and Co layers in $\text{Li}_{2/3}\text{CoO}_2$ at low temperatures. Both Li^+ and Co^{3+} ions form a honeycomb lattice (HCL) after slow cooling, whereas Li^+ ions enter a glass-like state with an amorphous structure accompanied by the disordered $\text{Co}^{3+}/\text{Co}^{4+}$ arrangement after rapid cooling. The glass-like state is followed by a supercooled liquid (SCL) state. (b) Plots of T_S , T_{F1} and T_{F2} vs Li content x . T_{MN} and T_d^{Li} , which indicate the onset temperature of the Li diffusion determined by the other group^{34,35}, are also plotted. In the blue-shaded area, an insulating behavior is observed in the measurements of electrical resistivity. The CO2/3 state ($\text{Co}^{3+}:\text{Co}^{4+} = 2 : 1$) appears together with an excess of Co^{3+} ions for $2/3 < x < 1$, while the CO1/2 state ($\text{Co}^{3+}:\text{Co}^{4+} = 1 : 1$) appears at $x \sim 1/2$. These CO states are thought to coexist for a certain x range around $x \sim 0.55$.

for $0.73 \leq x \leq 1.0$ ($0.6 \leq x \leq 0.98$). In Fig. 5(b), we also plot T_{MN} and T_d^{Li} determined by ^7Li NMR³⁴ and $\mu^+\text{SR}$ experiments³⁵, respectively, above which Li ions start diffusing. We note here that T_{MN} for $x=0.8$ has been observed only for hexagonal phase (I),³⁴ so that T_{MN} has a single value even in the two-phase region. T_{MN} and T_d^{Li} are shown to be consistent with T_{F1} and T_{F2} . Finally, we discuss how the charge ordering changes with decreasing x from $x=2/3$, since an appearance of the CO1/2 state

is expected at $x \sim 0.5$. The important point to note is the anomalous behaviors at $x = 0.55$, where T_S is fairly enhanced and the anomaly at T_{F2} is absent in the $\rho(T)$ and $M(T)$ curves. The most plausible scenario is that the CO2/3 state survives with an excess of Co^{4+} for $x < 2/3$, but the CO1/2 state begins to coexist below certain x and competes with the CO2/3 state near $x = 0.55$, and then the CO1/2 state becomes dominant for $x \sim 1/2$. Due to the competition between the CO2/3 and CO1/2 states, both arrangements of Li^+ and $\text{Co}^{3+}/\text{Co}^{4+}$ could be disordered even after slow cooling. Under the circumstance, we may expect either that Li ions do not undergo the transition at T_{F2} or that the arrangement of $\text{Co}^{3+}/\text{Co}^{4+}$ remains disordered even across T_{F2} . In both cases, no anomaly would be observed at T_{F2} . Assuming that all $\text{Co}^{3+}/\text{Co}^{4+}$ ions contribute to either CO1/2 or CO2/3 domains, the critical value of x at which the occupied area by the CO1/2 and CO2/3 states is totally equivalent (i.e., the molar fraction $p^{\text{CO1/2}} : p^{\text{CO2/3}} = 3 : 2$) is estimated to be $7/12 \sim 0.583$. The value is close to 0.55. The elucidation for the CO1/2 state and the ordering of Li ions at $x = 0.5$ by the combined study of the STM observation and DFT calculation must be the important step to understand the overall feature of Li_xCoO_2 .

IV. SUMMARY

In the present paper, we have investigated the low temperature magnetic and electrical properties of Li_xCoO_2 ($0.51 \leq x \leq 1.0$) using single-crystal specimens. The CO2/3 state has been found to appear in the wide x range $0.60 \leq x \leq 0.98$. In the powder XRD measurements,

we have observed mixed hexagonal phases (I) and (II) for $0.71 \leq x \leq 0.91$, each of which has a different lattice parameter c , in other words, different Li content. Taking also the results of the $\rho(T)$ and $M(T)$ measurements into account, it is suggested that the composition of phase (I) [phase (II)] is nearly LiCoO_2 ($\text{Li}_{2/3}\text{CoO}_2$), where the Li ions start diffusing above $T_{F1} \sim 370$ K ($T_{F2} \sim 120$ K). Furthermore, we have successfully observed that the $\rho(T)$ curves are fairly enhanced after rapid cooling of the specimens below $T_S \sim 155$ K, as an evidence of the occurrence of the disordered $\text{Co}^{3+}/\text{Co}^{4+}$ arrangement with an insulating electronic structure, which is led by an amorphous-like formation of Li ions. It is inferred that the CO1/2 state, which has an arrangement with $\text{Co}^{3+} : \text{Co}^{4+} = 1 : 1$, is realized at $x \sim 1/2$ and competes with the CO2/3 state for a certain x range around $x = 0.55$. We have also suggested that the state after rapid cooling between T_{F2} and T_S can be regarded as a supercooled liquid state as seen in metallic glass materials. Finally, we should note that Li_xCoO_2 is a high energy cathode material for Li ion batteries, but also an electron system, which provides us a great opportunity to encounter unique low-temperature properties related to the Li ion dynamics, being a potential material to exhibit a rapid-cooling-induced giant resistivity which is led by a different mechanism. Great attention should be paid to the progress of these studies.

Acknowledgments

The authors thank H. Katsube and K. Mihara for their technical assistance.

-
- ¹ J. B. Goodenough and Y. Kim, Chem. Mater. **22**, 587 (2010).
 - ² N. Nitta, F. Wu and J. T. Lee, G. Yushin, Mater. Today **18**, 587 (2015).
 - ³ I. Terasaki, Y. Sasago, and K. Uchinokura, Phys. Rev. B **56**, R12685 (1997).
 - ⁴ K. Takeda, H. Sakurai, E. Takayama-Muromachi and F. Izumi, Nature **422**, 53 (2003).
 - ⁵ M. L. Foo, Y. Wang, S. Watauchi, H. W. Zandbergen, T. He, R. J. Cava and N. P. Ong, Phys. Rev. Lett. **92**, 247001 (2004).
 - ⁶ M. Yokoi, T. Moyoshi, Y. Kobayashi, M. Soda, Y. Yasui, M. Sato, and K. Kakurai, J. Phys. Soc. Japan **74**, 3046 (2005).
 - ⁷ G. Gaspárović, R. A. Ott, J. -H. Cho, F. C. Chou, Y. Chu, J. W. Lynn and Y. S. Lee, Phys. Rev. Lett. **96**, 046403 (2006).
 - ⁸ F. L. Ning, S. M. Golin, K. Ahilan, T. Imai, G. J. Shu, and F. C. Chou, Phys. Rev. Lett. **100**, 086405 (2008).
 - ⁹ K. Miyoshi, E. Morikuni, K. Fujiwara, J. Takeuchi, and T. Hamasaki, Phys. Rev. B **69**, 132412 (2004).
 - ¹⁰ T. Motohashi, R. Ueda, E. Naujalis, T. Tojo, I. Terasaki, T. Atake, M. Karppinen, and H. Yamauchi, Phys. Rev. B **67**, 064406 (2003).
 - ¹¹ H. W. Zandbergen, M. L. Foo, Q. Xu, V. Kumar, and R. J. Cava, Phys. Rev. B **70**, 024101 (2004).
 - ¹² F. C. Chou, M. -W. Chu, G. J. Shu, F.-T. Huang, W. W. Pai, H. S. Sheu, and P. A. Lee, Phys. Rev. Lett. **101**, 127404 (2008).
 - ¹³ M. Weller, A. Sacchetti, H. R. Ott, K. Mattenberger, and B. Batlogg, Phys. Rev. Lett. **102**, 056401 (2009).
 - ¹⁴ Y. S. Meng, A. Van der Ven, M. K. Y. Chan, and G. Ceder, Phys. Rev. B **72**, 172103 (2005).
 - ¹⁵ M. Roger, D. J. P. Morris, D. A. Tennant, M. J. Gutmann, J. P. Goff, J.-U. Hoffmann, R. Feyerherm, E. Dudzik, D. Prabhakaran, A. T. Boothroyd, N. Shannon, B. Lake, and P. P. Deen, Nature (London) **445**, 631 (2007).
 - ¹⁶ M. -H. Julien, C. de Vaulx, H. Mayaffre, C. Berthier, M. Horvatić, V. Simonet, J. Wooldridge, G. Balakrishnan, M. R. Lees, D. P. Chen, C. T. Lin, and P. Lejay, Phys. Rev. Lett. **100**, 096405 (2008).
 - ¹⁷ D. J. P. Morris, M. Roger, M. J. Gutmann, J. P. Goff, D. A. Tennant, D. Prabhakaran, A. T. Boothroyd, E. Dudzik, R. Feyerherm, J.-U. Hoffmann, and K. Kiefer, Phys. Rev. B **79**, 100103(R) (2009).
 - ¹⁸ H. Alloul, I. R. Mukhamedshin1, T. A. Platova1, and A.

- V. Dooglav, EuroPhys. Lett. **85**, 47006 (2009).
- ¹⁹ I. R. Mukhamedshin, A. V. Dooglav, S. A. Krivenko, and H. Alloul, Phys. Rev. B **90**, 115151 (2014).
 - ²⁰ T. F. Schulze, P. S. Häfliger, Ch. Niedermayer, K. Mattenberger, S. Bubenhofer, and B. Batlogg, Phys. Rev. Lett. **100**, 026407 (2008).
 - ²¹ M. Medarde, M. Mena, J. L. Gavilano, E. Pomjakushina, J. Sugiyama, K. Kamazawa, V. Yu. Pomjakushin, D. Sheptyakov, B. Batlogg, H. R. Ott, M. Mansson, and F. Jurnani, Phys. Rev. Lett. **110**, 266401 (2013).
 - ²² S. Galeski, K. Mattenberger, and B. Batlogg, Phys. Rev. B **94**, 140402(R) (2016).
 - ²³ R. Ray, A. Ghoshray, K. Ghoshray, and S. Nakamura, Phys. Rev. B **59**, 9454 (1999).
 - ²⁴ M. Ménétrier, I. Saadoun, S. Levasseur, and C. Delmas, J. Mater. Chem. **9**, 1135 (1999).
 - ²⁵ D. G. Kellerman, V. R. Galakhov, A. S. Semenove, Ya. N. Blinnskov, and O. N. Leonidova, Phys. Solid State **48**, 548 (2006).
 - ²⁶ K. Miyoshi, C. Iwai, H. Kondo, M. Miura, S. Nishigori, and J. Takeuchi, Phys. Rev. B **82**, 075113 (2010).
 - ²⁷ T. Motohashi, Y. Sugimoto, Y. Masubuchi, T. Sasagawa, W. Koshibae, T. Tohyama, H. Yamauchi, and S. Kikkawa, Phys. Rev. B **83**, 195128 (2011).
 - ²⁸ Q. Lin, Q. Li, K. E. Gray, and J. F. Mitchell, J. Cryst. Growth Des. **12**, 1232 (2012).
 - ²⁹ J. Sugiyama, H. Nozaki, J. H. Brewer, E. J. Ansaldo, G. D. Morris, and C. Delmas, Phys. Rev. B **72**, 144424 (2005).
 - ³⁰ K. Mukai, Y. Ikeda, H. Nozaki, J. Sugiyama, K. Nishiyama, D. Andreica, A. Amato, P. L. Russo, E. J. Ansaldo, J. H. Brewer, K. H. Chow, K. Ariyoshi, and T. Ohzuku, Phys. Rev. Lett. **99**, 087601 (2007).
 - ³¹ J. T. Hertz, Q. Huang, T. McQueen, T. Klimczuk, J. W. G. Bos, L. Viciu, and R. J. Cava, Phys. Rev. B **77**, 075119 (2008).
 - ³² T. Motohashi, T. Ono, Y. Sugimoto, Y. Masubuchi, S. Kikkawa, R. Kanno, M. Karppinen, and H. Yamauchi, Phys. Rev. B **80**, 165114 (2009).
 - ³³ K. Iwaya, T. Ogawa, T. Minato, K. Miyoshi, J. Takeuchi, A. Kuwabara, H. Moriwake, Y. Kim, and T. Hitosugi, Phys. Rev. Lett. **111**, 126104 (2013).
 - ³⁴ K. Nakamura, H. Ohno, K. Okamura, Y. Michihiro, T. Moriga, I. Nakabayashi, and T. Kanashiro, Solid State Ionics **177**, 821 (2006).
 - ³⁵ J. Sugiyama, K. Mukai, Y. Ikeda, H. Nozaki, M. Mansson, and I. Watanabe, Phys. Rev. Lett. **103**, 147601 (2009).
 - ³⁶ K. Ikeda, Y. Wakisaka, T. Mizokawa, C. Iwai, K. Miyoshi, and J. Takeuchi, Phys. Rev. B **82**, 075126 (2010).
 - ³⁷ T. Mizokawa, Y. Wakisaka, T. Sudayama, C. Iwai, K. Miyoshi, J. Takeuchi, H. Wadati, D. G. Hawthorn, T. Z. Regier, and G. A. Sawatzky, Phys. Rev. Lett. **111**, 056404 (2013).
 - ³⁸ L. Simonelli, E. Paris, C. Iwai, K. Miyoshi, J. Takeuchi, T. Mizokawa, and N. L. Saini, J. Phys.:Condens. Matter **29**, 105702 (2017).
 - ³⁹ Y. Okamoto, R. Matsumoto, T. Yagihara, C. Iwai, K. Miyoshi, J. Takeuchi, K. Horiba, M. Kobayashi, K. Ono, H. Kumigashira, N. L. Saini, and T. Mizokawa, Phys. Rev. B **96**, 125147 (2017).
 - ⁴⁰ F. C. Chou, J. H. Cho, P. A. Lee, E. T. Abel, K. Matan, and Y. S. Lee, Phys. Rev. Lett. **92**, 157004 (2004).
 - ⁴¹ J. N. Reimers and J. R. Dahn, J. Electrochem. Soc. **139**, 2091 (1992).
 - ⁴² T. Ohzuku and A. Ueda, J. Electrochem. Soc. **141**, 2972 (1994).
 - ⁴³ G. G. Amatucci, J. M. Tarascon, and L. C. Klein, J. Electrochem. Soc., **143**, 1114 (1996).
 - ⁴⁴ Y. Ishida, A. Mizutani, K. Sugiura, H. Ohta, and K. Koumoto, Phys. Rev. B **82**, 075325 (2010).
 - ⁴⁵ Generally, layered oxides $A_x\text{CoO}_2$ (A =alkali metal) have a tendency to have a larger lattice constant c for smaller x , because the interlayer Coulomb interactions are reduced and the interlayer distance is increased with decreasing the concentration of alkali ions.
 - ⁴⁶ H. Oike, F. Kagawa, N. Ogawa, A. Ueda, H. Mori, M. Kawasaki, and Y. Tokura, Phys. Rev. B **91**, 041101(R) (2015).
 - ⁴⁷ F. Kagawa and H. Oike, Adv. Mater. **29**, 1601979 (2017).
 - ⁴⁸ T. Zhang, A. Inoue, and T. Masumoto, Mater. Trans., JIM, **32**, 1005 (1991).
 - ⁴⁹ A. Peker and W. L. Johnson, Appl. Phys. Lett. **63**, 2342 (1995).